Heterogeneous Nucleation Experiments Bridging the Scale from Molecular Ion Clusters to Nanoparticles

Paul M. Winkler, *et al.*

Science **319**, 1374 (2008);
DOI: 10.1126/science.1149034

a physiological temperature of 37°C at ~2°C/min (*30*) (Movie S1), leads to a pronounced reduction of E'. Whereas the neat PVAc (dry E'_s = 1.8 GPa at 25°C) instantly softens under these conditions (Fig. 4B), the E' of the whisker-reinforced nanocomposites (see Fig. 4B for a 12.2% v/v nanocomposite) is reduced slowly over a period of 15 min. The whisker-reinforced nanocomposite displays a much higher dry E' (4.2 GPa at 25°C) than the neat PVAc, but both materials reach nearly identical moduli upon immersion in ACSF at 37°C (1.6 MPa).

Our data support a simple and versatile strategy for the creation of polymer nanocomposites, whose architecture and mechanical adaptability closely mimic the proposed architecture and observed response of the sea cucumber dermis. The mechanical properties of these chemoresponsive materials can selectively and reversibly be controlled through the formation and decoupling of a three-dimensional network of well-individualized nanofibers in response to specific chemical triggers. It will be interesting to explore whether the framework can be adapted to nonchemical triggers, for example, optical or electrical stimuli.

References and Notes

1. T. Heinzeller, J. Nebelsick, Eds., *Echinoderms* (Taylor & Francis, London, **2004**).
2. T. Motokawa, *Comp. Biochem. Physiol. B* **109**, 613 (1994).
3. F. A. Thurmond, J. A. Trotter, *J. Exp. Biol.* **199**, 1817 (1996).
4. I. C. Wilkie, *J. Exp. Biol.* **205**, 159 (2002).
5. J. A. Trotter, T. J. Koob, *Matrix Biol.* **18**, 569 (1999).
6. G. K. Szulgit, R. E. Shadwick, *J. Exp. Biol.* **203**, 1539 (2000).
7. J. A. Trotter *et al.*, *Biochem. Soc. Trans.* **28**, 357 (2000).
8. J. C. Grunlan, L. Liu, Y. S. Kim, *Nano Lett.* **6**, 911 (2006).
9. M. M. de Souza Lima, R. Borsali, *Macromol. Rapid Commun.* **25**, 771 (2004).
10. J. A. Jaber, J. B. Schlenoff, *J. Am. Chem. Soc.* **128**, 2940 (2006).
11. D. M. Loveless, S. L. Jeon, S. L. Craïg, *J. Mater. Chem.* **17**, 56 (2007).
12. P. S. Belton, S. F. Tanner, N. Cartier, H. Chanzy, *Macromolecules* **22**, 1615 (1989).
13. A. Sturcova, J. R. Davies, S. J. Eichhorn, *Biomacromolecules* **6**, 1055 (2005).
14. O. van den Berg, J. R. Capadona, C. Weder, *Biomacromolecules* **8**, 1353 (2007).
15. M. A. S. Azizi Samir, F. Alloin, A. Dufresne, *Biomacromolecules* **6**, 612 (2005).
16. J. R. Capadona *et al.*, *Nat. Nanotech.* **2**, 765 (2007).
17. M. Takayanagi, S. Uemura, S. Minami, *J. Polym. Sci. C* **5**, 113 (1964).
18. N. Ouali, J. Y. Cavaillé, J. Pérez, *J. Plast. Rubber Comp. Process. Appl.* **16**, 55 (1991).
19. Swelling increased the volume of the nanocomposites and reduced the volume fraction of whiskers, X_r. For example, when a nanocomposite with X_r = 19% v/v was swollen with water, X_r decreased to 14%. The representation of data in Fig. 2A considers this effect to allow for analysis by the Halpin-Kardos model. A direct comparison of dry versus wet composites for the same fiber loading is shown in fig. S6.
20. J. Kunzelman, B. R. Crenshaw, C. Weder, *J. Mater. Chem.* **17**, 2989 (2007).
21. J. C. Halpin, J. L. Kardos, *J. Appl. Phys.* **43**, 2235 (1972).
22. P. Hajji, J. Y. Cavaillé, V. Favier, C. Gauthier, G. Vigier, *Polym. Compos.* **17**, 612 (1996).
23. $\eta_L = [(E_{lr} / E'_s) - 1]/[(E_{lr} / E'_s) + 2A]$, and $\eta_T = [(E_{tr} / E'_s) - 1]/[(E_{tr} / E'_s) + 2]$. A is the aspect ratio of the whiskers, ϕ is equal to the volume fraction of the phase, and the subscripts s and r represent the soft phase and the rigid phase, respectively. E_{lr} is the longitudinal Young's Modulus (130 GPa), and E_{tr} is the transverse Young's Modulus (5 GPa) of an individual cellulose whisker (*22*). To determine the tensile storage modulus of the isotropic nanocomposite (E'), E'_L and E'_T must be inserted into one equation using the Halpin-Kardos model: $E' = 4U_5(U_1 - U_5)/U_1$ where $U_1 = 1/8(3Q_{11} + 3Q_{22} + 4Q_{66})$; $U_5 = 1/8(Q_{11} + Q_{22} - 2Q_{12} + 4Q_{66})$; $Q_{11} = E'_L/(1 - \nu_{12}\nu_{21})$; $Q_{22} = E'_T(1 - \nu_{12}\nu_{21})$; $Q_{12} = \nu_{12}Q_{22} = \nu_{21}Q_{11}$; $Q_{66} = G_{12}$; $\nu_{12} = \phi_r\nu_r + \phi_s\nu_s = 0.3$; $G_{12} = G_s(1 + \eta\phi_r)/(1 - \eta\phi_r)$; $\eta = (G_r/G_s - 1)/(G_r/G_s + 1)$, ν is the Poisson's ratio, G is the shear modulus, and G_r = 1.77 GPa.
24. D. M. Taylor, S. I. H. Tillery, A. B. Schwartz, *Science* **296**, 1829 (2002).
25. A. B. Schwartz, *Annu. Rev. Neurosci.* **27**, 487 (2004).
26. R. Biran, D. C. Martin, P. A. Tresco, *J. Biomed. Mater. Res.* **82A**, 169 (2007).
27. W. L. C. Rutten, *Annu. Rev. Biomed. Eng.* **4**, 407 (2002).
28. D. H. Szarowski *et al.*, *Brain Res.* **983**, 23 (2003).
29. K. Najafi, J. F. Hetke, *IEEE Trans. Biomed. Eng.* **37**, 474 (1990).
30. Materials and methods are available as supporting material on *Science* Online.

31. We thank F. Carpenter for the photography of the sea cucumber and L. McCorkle, J. Johnson, and M. Hitomi for assistance with the SEM, AFM, and TEM experiments, respectively. Financial support from DuPont (Young Professor Award to C.W.), the L. Stokes Cleveland VAMC Advanced Platform Technology Center, an Ohio Innovation Incentive Fellowship (to K.S.), the Department of Veterans Affairs Associate Investigator Career Development Program (to J.C.), and the National Institutes of Health are gratefully acknowledged. The authors declare that they have no competing financial interest.

Supporting Online Material

www.sciencemag.org/cgi/content/full/319/5868/1370/DC1
Materials and Methods
Figs. S1 to 10
Table S1
References
Movie S1

6 November 2007; accepted 1 February 2008
10.1126/science.1153307

Heterogeneous Nucleation Experiments Bridging the Scale from Molecular Ion Clusters to Nanoparticles

Paul M. Winkler,[1] Gerhard Steiner,[1] Aron Vrtala,[1] Hanna Vehkamäki,[2] Madis Noppel,[3] Kari E. J. Lehtinen,[4] Georg P. Reischl,[1] Paul E. Wagner,[1] Markku Kulmala[2]*

Generation, investigation, and manipulation of nanostructured materials are of fundamental and practical importance for several disciplines, including materials science and medicine. Recently, atmospheric new particle formation in the nanometer-size range has been found to be a global phenomenon. Still, its detailed mechanisms are mostly unknown, largely depending on the incapability to generate and measure nanoparticles in a controlled way. In our experiments, an organic vapor (*n*-propanol) condenses on molecular ions, as well as on charged and uncharged inorganic nanoparticles, via initial activation by heterogeneous nucleation. We found a smooth transition in activation behavior as a function of size and activation to occur well before the onset of homogeneous nucleation. Furthermore, nucleation enhancement for charged particles and a substantial negative sign preference were quantitatively detected.

Condensational growth, evaporation, and heterogeneous chemistry are important phenomena in materials science, fluid dynamics, aerosol physics and technology, and atmospheric chemistry, including cloud microphysics and cloud chemistry. A prerequisite for the start of condensation is homogeneous nucleation of new particles or the activation of preexisting particles by heterogeneous nucleation. The latter can occur either on ions, soluble particles, or insoluble particles, and is energetically easier than homogeneous nucleation (*1*). Both particle formation processes are of fundamental as well as practical importance and have been the subject of investigations for more than a century (*2*). Important examples representing the different processes are given by the use of the Wilson cloud chamber (*3*) in high-energy physics for the case of ions, the formation of cloud droplets in the troposphere for the case of soluble particles, and the occurrence of ice nucleation for the case of insoluble seed particles (*4*). Atmospheric observations suggest that the initial formation and growth are two uncoupled processes (*5*–*7*), and therefore the activation mechanism of small clusters is of vital importance. Understanding the formation and initial growth processes in detail is also crucial to control the production of nanomaterials (*8*).

In this paper, we present experimental results for the activation of molecular cluster ions, charged and neutral clusters, and nanometer-size particles having almost monodisperse size distributions,

[1]Fakultät für Physik, Universität Wien, Boltzmanngasse 5, A-1090 Wien, Austria. [2]University of Helsinki, Department of Physical Sciences, Post Office Box 64, 00014 University of Helsinki, Finland. [3]Institute of Physics, University of Tartu, 18 Ülikooli Street, 50090 Tartu, Estonia. [4]Department of Physics, University of Kuopio and Finnish Meteorological Institute, Post Office Box 1627, 70211 Kuopio, Finland.

*To whom correspondence should be addressed. E-mail: markku.kulmala@helsinki.fi

with mean diameters ranging from 1 to 24 nm and geometric SDs between 1.021 and 1.058. Particle number concentrations were between 2000 and 10,000 cm^{-3}. We used insoluble inorganic seed aerosol (WO_x) and condensable organic vapor (*n*-propanol) to determine the dependence of activation diameter on charging state and vapor saturation ratio. For comparison, other insoluble inorganic seed aerosols [Ag and $(NH_4)_2SO_4$] were also used (*9*). The range of particle sizes studied—together with the fact that the particles are, in practice, monodispersed—is the main novelty of our work: To our knowledge, this is the first time that activation of neutral particles has been studied for particles smaller than 3 nm in diameter.

The experimental system (*9*) includes a source of monodispersed particles and a vapor generation unit. Vapor supersaturation is achieved by adiabatic expansion in a computer-controlled thermostated expansion chamber [the size-analyzing nuclei counter (SANC)]. Droplet growth is observed by means of the constant-angle Mie scattering (CAMS) detection method (*10*). Details of the experimental system are presented elsewhere (*11*).

We generated well-defined nearly monodispersed nanoparticles using different types of particle generators in combination with an electrostatic classification system capable of selecting particles with specified charging state and mobility diameters down to and even below 1 nm. Ions were obtained from a radioactive source in a ^{241}Am charger. Charged particles leaving the classifier were either passed through a ^{241}Am neutralizer to obtain neutral particles or passed by the neutralizer to preserve charging properties. In order to remove ions, which were produced in the neutralizer, from the aerosol flow, we applied an ion trap. *n*-Propanol vapor was added to the system by controlled injection of a liquid beam and subsequent quantitative evaporation in a heated unit. Those particles inducing heterogeneous nucleation in the SANC expansion chamber at the vapor supersaturations considered lead to the formation and growth of liquid droplets, which were optically detected.

We measured heterogeneous nucleation (activation) probabilities using the above described SANC-CAMS method. For all experiments reported in this paper, the nucleation temperature was kept constant at about 275 K. For each *n*-propanol vapor saturation ratio, the fraction of activated particles relative to total particle number concentration was determined, resulting in a nucleation-activation probability curve. Experimental nucleation probabilities, determined for molecular ions and nanometer-size particles, are shown in Fig. 1. The diameters of the seed objects range from 4 nm down to 0.9 nm. The smaller the size, the higher the saturation ratio that is needed for activation, reflecting the well-known curvature effect first observed by Thomson (*12*). As can be seen, at 4 nm, the nucleation probability curves are mainly overlapping, whereas with decreasing particle size, the curves split up, indicating that charge effects increasingly promote the nucleation process. Negatively charged particles are found to require smaller saturation ratios to activate for nucleation than positively charged particles and neutral ones.

Each probability curve can be represented by the corresponding onset saturation ratio (i.e., the saturation ratio where 50% of the particles of a certain size are activated). Experimental onset saturation ratios as functions of mobility diameter, together with the Kelvin diameter and the homogeneous nucleation limit, are shown in Fig. 2. The Kelvin diameter corresponds to the size at which the vapor and aerosol particles, whose surfaces are coated with *n*-propanol, are in equilibrium (*9*). In principle, if the particle size is larger than the Kelvin diameter, the aerosol particles will grow; if the particle size is smaller, they will evaporate. However, in our experiments, all particles considered are activated and start to grow at sizes clearly smaller than those indicated by the Kelvin equation and at saturation ratios well below the onset of homogeneous nucleation.

For particles with diameters around 4 nm and above, nucleation behavior was found to be independent of charging state. However, as seen already in Fig. 1, charge effects become increasingly important with decreasing particle size. Differences between heterogeneous nucleation on charged and neutral particles were experimentally observed, starting at diameters below 3 nm. Clearly, a "sign effect" can be seen, meaning that negatively charged particles appear to be more easily activated for growth than positively charged particles. Smaller saturation ratios are generally required to activate charged particles for nucleation. For example, at a saturation ratio of 2.75, the activation size is 1.4 nm for negative clusters and 1.8 nm for neutral ones. A smooth transition from molecular ions to particles is observed, thereby bridging the scale from molecular ion clusters to nanoparticles. Consistently, for ions, a similar sign effect has been found as for charged particles. Recently, Nadykto *et al.* (*13*) have proposed that the sign can be reproduced by quantum chemical methods and may be positive or negative, depending on the nature of the ions considered.

In Fig. 2, we also compare our experimental findings with an onset activation curve predicted by heterogeneous nucleation theory (*9*, *14*). In heterogeneous nucleation, the critical cluster is formed on a preexisting surface, and only part of the vapor-liquid surface needs to be built from scratch, because part of it can be borrowed from the preexisting interface; this fact decreases the energy barrier of cluster formation as compared with homogeneous nucleation (*1*, *11*). The angle between the preexisting surface and the surface of the nucleating cluster is called the contact angle θ. The value that we used for the contact angle was 0°, corresponding to the recent observations for *n*-propanol droplets nucleating on an Ag surface (*11*). Substantially larger contact angles would lead to a predicted activation diameter being larger than the Kelvin diameter (*1*), which is in contrast to our experimental findings; thus, we conclude that the particles are, in practice, totally wettable to the *n*-propanol vapor. In atmospheric and materials science, heterogeneous nucleation is typically ignored. This is mainly because no proper experimental data have so far existed at particle sizes small enough to be relevant to formation and initial growth. Our results, however, show that the theory developed by Fletcher 50 years ago predicts the observed onset activations for neutral particles and clusters exceedingly well, even at the size range of small molecular clusters.

The effect of charge on the onset activation curves can be estimated by ion-induced nucleation theory—with Gibbs free energies calculated based on the Thomson theory (*15*)—together with the Fletcher theory (*9*), hereafter referred to as the "combined" theory. The onset activation satura-

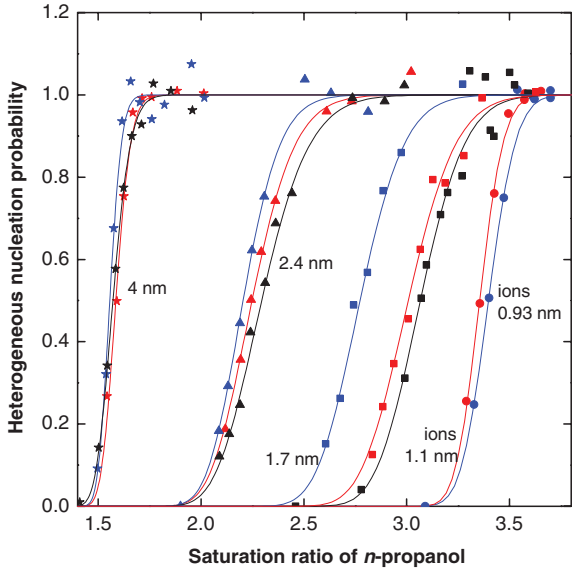

Fig. 1. Heterogeneous nucleation probabilities versus vapor saturation ratio for nucleation of *n*-propanol on ions as well as charged and uncharged WO_x clusters of different diameters: WO_x, 4 nm (stars); WO_x, 2.4 nm (triangles); WO_x, 1.7 nm (squares); positive ions, 1.1 nm (red circles); and negative ions, 0.93 nm (blue circles). Colors refer to different charging states: blue (negatively charged), red (positively charged), and black (neutral). Solid lines are shown to guide the eye.

tion ratio as a function of diameter, estimated by the combined theory, is also superimposed in Fig. 2, showing an even lower supersaturation required for activation. The combined theory provides no explanation why negative particles activate before positive ones of the same size. However, the difference between the Fletcher theory (heterogeneous nucleation) and the combined theory (heterogeneous and ion-induced nucleation) seems to provide a useful estimate for the difference in onset activation supersaturations between charged and neutral particles.

The use of the recently developed heterogeneous nucleation theorem (*16*) will provide an estimation of the number of molecules in the nucleating cluster. In the experiments presented here, the number is around 20 to 25 molecules. The ratio of the experimental activation diameter to the Kelvin diameter is almost size-independent and is around 0.65. Our experimental technique can thus be used to produce particles, with a well-defined surface layer consisting of a small number of molecules, for future technical and industrial purposes.

So far, it has been generally accepted (*1*, *17*) that activation of (neutral) particles is predicted by the Kelvin equation. The fact that particles are activated at much smaller sizes than indicated by the Kelvin equation is thus unexpected; apparently, heterogeneous nucleation has been typically forgotten or at least ignored, and the Fletcher theory has not been applied to small clusters or nanoparticles. The latest findings will give insight to some aspects of materials science, atmospheric particle formation, and especially to measurement techniques of small aerosol particles. Based on laboratory experiments, atmospheric observations, and modeling (*18*–*20*), it is often predicted that homogeneous nucleation will produce particles with diameters around 1 to 2 nm. Indeed, Strey *et al*. (*21*) have shown that, for the case of homogeneous nucleation (i.e., in the absence of seed particles), the critical cluster size agrees well with the Kelvin equation; this indicates that the Kelvin equation remains generally valid for critical clusters down to the size range of 1 to 2 nm. Our results show that, for example, if the Kelvin diameter is 2 nm, then the activation diameter is around 1.2 nm; this finding indicates that all seed particles with diameters larger than 1.2 nm are capable of acting as nuclei for condensation, which is also consistent with the recent observation of size-dependent aerosol growth (*6*). As described by the Fletcher theory (*9*, *14*), small embryos have a thermodynamic barrier to cross, but critical size clusters are nevertheless formed on seed particles as a result of statistical fluctuations. They reach the critical size and become stable for growth when their radius coincides with the Kelvin curvature. The work of formation of an embryo on a seed particle is always smaller than the work of formation of a Kelvin-size embryo in homogeneous nucleation, even if the seed particle diameter is below the Kelvin size. This is manifested by our finding that organic vapor will condense much easier on even the smallest preexisting seed particles than form new particles.

In nanomaterial production, there are several examples of experiments where the detailed particle formation, activation, and/or initial growth mechanisms are unknown, and modeling attempts have been unsuccessful (*22*, *23*). These modeling efforts are typically based on the application of classical homogeneous nucleation theory with some adjustable factor, together with coagulation and condensation models for the growth. The heterogeneous nucleation-activation stage is typically neglected, and condensation is assumed to start at the Kelvin limit. The present study proposes one severe deficiency in these approaches, because we clearly observe that activation and condensational growth can start at sizes significantly smaller than previously expected from the Kelvin equation.

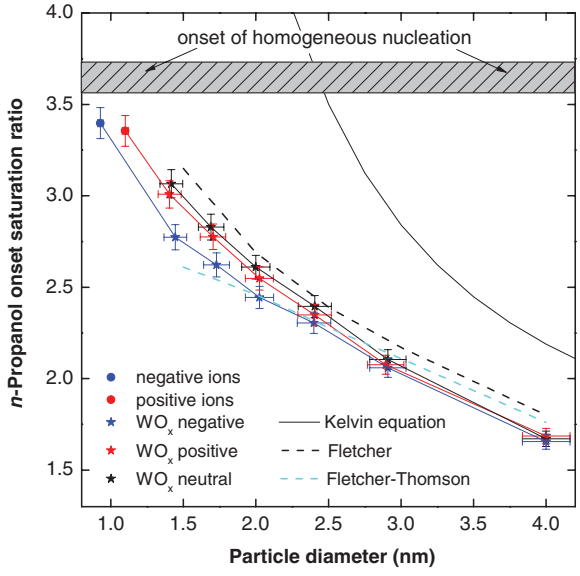

Fig. 2. Experimental onset saturation ratio as a function of seed particle mobility diameter for ions as well as for charged and uncharged WO_x particles. The Kelvin diameter (solid black line) and the homogeneous nucleation onset [cross-hatched shaded area (*29*)] are shown for comparison. We also show the predictions by the Fletcher theory for heterogeneous nucleation on uncharged particles (dashed black line) and the combined theory accounting for the charge of the seed particles (dashed cyan line) (*9*). Error bars indicate the measurement uncertainty when measuring saturation ratio and particle diameter.

One of the main implications of this study is that the detection limit of condensation particle counters (CPCs) can be extended to considerably smaller sizes (*24*, *25*). The operating principle of these devices is based on activation of particles in supersaturated vapors and consequent growth to sizes detectable by optical methods. A major concern has been possible homogeneous nucleation of new particles when the application of high supersaturations is required to activate nanoparticles. However, this study shows that, rather than nucleating homogeneously to form new particles, the vapors tend to nucleate heterogeneously and further condense onto the preexisting particles at sizes much smaller than believed in the past. This fact has already been used in atmospheric studies (*1*).

In the literature, there are some laboratory studies concerning the effect of ions on the nucleation rate. However, they are not typically related to activation of existing particles or clusters. For example, Kim *et al*. (*26*) investigated homogeneous and ion-induced nucleation in the ternary $NH_3/SO_2/H_2O$/air mixture. As a result of their study, they proposed that the main particle production mechanism is homogeneous nucleation of $(NH_4)_2SO_4$ molecules produced by the H_2SO_4-NH_3 reaction. Several years ago, Gamero-Castaño and de la Mora (*17*) proposed clusters as "impurities in the gas phase" using their CPC. Their study focused on the activation of ions and charged nanoclusters with the use of a CPC, but did not include any comparison between charged and neutral particles.

The presence of ions, and electric charge on particles, will enhance not only the activation probabilities but also the growth rates of very small (nanometer-size) aerosol particles and air ions (*27*, *28*). The condensing vapors may exhibit dipole nature and can thus be electrostatically attracted to charged particles. This effect decreases rapidly with increasing particle size, which means that if this mechanism dominates the growth of freshly nucleated particles, the particle growth rate should decrease as a function of the particle size. However, no sign of such a growth dependence has been reported. Although the condensation enhancement factor caused by the presence of electric charges varies between the different theories, all of the theories predict a fairly similar size dependence for this effect (*6*). However, according to our present study, the possible difference in growth has a much smaller effect on atmospheric aerosol formation than the activation probability. Therefore, we can conclude that the key process in atmospheric investigations is the activation of preexisting clusters and nanoparticles.

From the point of view of atmospheric aerosols and their climate interaction, our observation allows a more accurate description of cluster activation leading to aerosol formation. In atmospheric processes, several different organic compounds are undoubtedly participating in the activation process.

References and Notes

1. M. Kulmala *et al.*, *J. Aerosol Sci.* **38**, 289 (2007).
2. C. T. R. Wilson, *Philos. Trans. R. Soc. London Ser. A* **189**, 265 (1897).
3. N. N. Das Gupta, S. K. Ghosh, *Rev. Mod. Phys.* **18**, 225 (1946).
4. H. R. Pruppacher, J. D. Klett, *Microphysics of Clouds and Precipitation* (Kluwer Academic, Dordrecht, Netherlands, 1997).
5. M. Kulmala, L. Pirjola, J. M. Mäkelä, *Nature* **404**, 66 (2000).
6. M. Kulmala *et al.*, *Atmos. Chem. Phys.* **4**, 2553 (2004).
7. M. Kulmala, K. E. J. Lehtinen, A. Laaksonen, *Atmos. Chem. Phys.* **6**, 787 (2006).
8. T. T. Kodas, M. J. Hampden-Smith, *Aerosol Processing of Materials* (Wiley-VCH, New York, 1999).
9. Detailed information on experimental methods, further results, and theory is available as supporting material on *Science* Online.
10. P. E. Wagner, *J. Colloid Interface Sci.* **105**, 456 (1985).
11. P. E. Wagner, D. Kaller, A. Vrtala, A. Lauri, M. Kulmala, *Phys. Rev. E Stat. Nonlin. Soft Matter Phys.* **67**, 021605 (2003).
12. W. Thomson, *Proc. R. Soc. Edinburgh* **7**, 63 (1870).
13. A. B. Nadykto, A. A. Natsheh, F. Yu, K. V. Mikkelsen, J. Ruuskanen, *Phys. Rev. Lett.* **96**, 125701 (2006).
14. N. Fletcher, *J. Chem. Phys.* **29**, 572 (1958).
15. M. Noppel, H. Vehkamäki, M. Kulmala, *J. Chem. Phys.* **119**, 10733 (2003).
16. H. Vehkamäki *et al.*, *J. Chem. Phys.* **126**, 174707 (2007).
17. M. Gamero-Castaño, J. F. de la Mora, *J. Aerosol Sci.* **31**, 757 (2000).
18. M. Kulmala, *Science* **302**, 1000 (2003).
19. M. Kulmala *et al.*, *J. Aerosol Sci.* **35**, 143 (2004).
20. D. Kashchiev, *Nucleation: Basic Theory with Applications* (Butterworth-Heinemann, Oxford, 2000).
21. R. Strey, P. E. Wagner, Y. Viisanen, *J. Phys. Chem.* **98**, 7748 (1994).
22. M. Wilck, F. Stratmann, *J. Aerosol Sci.* **28**, 959 (1997).
23. U. Backman, J. K. Jokiniemi, A. Auvinen, K. E. J. Lehtinen, *J. Nanoparticle Res.* **4**, 325 (2002).
24. P. H. McMurry, *Atmos. Environ.* **34**, 1959 (2000).
25. M. Kulmala, K. E. J. Lehtinen, L. Laakso, G. Mordas, K. Hämeri, *Boreal Environ. Res.* **10**, 79 (2005).
26. T. O. Kim, T. Ishida, M. Adachi, K. Okuyama, J. H. Seinfeld, *Aerosol Sci. Technol.* **29**, 111 (1998).
27. F. Yu, R. P. Turco, *Geophys. Res. Lett.* **27**, 883 (2000).
28. A. A. Lushnikov, M. Kulmala, *Eur. Phys. J. D* **29**, 345 (2004).
29. J. Wedekind, K. Iland, P. E. Wagner, R. Strey, in *Nucleation and Atmospheric Aerosols 2004*, M. Kasahara, M. Kulmala, Eds. (Kyoto Univ. Press, Kyoto, 2004), pp. 49–52.

30. This work was supported by the Austrian Science Foundation (Project No. P16958-N02 and P19546-N20), the Estonian Science Foundation (Grants 6223 and 6988), and the Academy of Finland. The authors declare no competing interests. Authors' contributions statement: experiments (P.M.W. and P.E.W.), nanoparticle generation (G.S., G.P.R., and P.M.W.), data analysis (P.M.W. and A.V.), theory and model calculations (M.K., M.N., H.V., and K.E.J.L.), writing (M.K., P.E.W., P.M.W., G.S., K.E.J.L., M.N., and H.V.).

Supporting Online Material

www.sciencemag.org/cgi/content/full/319/5868/1374/DC1
SOM Text
Figs. S1 to S5
Table S1
References

9 August 2007; accepted 24 January 2008
10.1126/science.1149034

Age and Evolution of the Grand Canyon Revealed by U-Pb Dating of Water Table–Type Speleothems

Victor Polyak,* Carol Hill, Yemane Asmerom

The age and evolution of the Grand Canyon have been subjects of great interest and debate since its discovery. We found that cave mammillaries (water table indicator speleothems) from nine sites in the Grand Canyon showed uranium-lead dating evidence for an old western Grand Canyon on the assumption that groundwater table decline rates are equivalent to incision rates. Samples in the western Grand Canyon yielded apparent water table decline rates of 55 to 123 meters per million years over the past 17 million years, in contrast to eastern Grand Canyon samples that yielded much faster rates (166 to 411 meters per million years). Chronology and inferred incision data indicate that the Grand Canyon evolved via headward erosion from west to east, together with late-stage (~3.7 million years ago) accelerated incision in the eastern block.

Ever since the first geologist known to set eyes on the Grand Canyon, John Strong Newberry in 1858, and the famous John Wesley Powell expedition of 1869 (*1*), the age and origin of the Grand Canyon have remained a subject of great scientific and popular interest. Accurate incision rate data have, until now, come from dating basalt flows and travertine deposits, but these results have not been able to record both the downward and headward incision of the Grand Canyon over its entire history beyond 1 million years ago (Ma) and higher than 100 m above the river (*2*). More than 50 years ago, Arthur Lange, a speleologist, proposed that the study of cave sediments and speleothems (cave formations) could produce an accurate minimum age for the Grand Canyon (*3*). U-series dating of speleothems, and consequently landscape evolution determinations using caves, began in the 1970s by alpha spectrometry (*4*) and were greatly improved by the application of mass spectrometry in the mid-1980s (*5*).

The realization that certain speleothems such as mammillary coatings (Fig. 1) form near groundwater tables [herein referred to as water tables (*6*)], and the fact that many Grand Canyon caves contain mammillary speleothems (*7*), has allowed us to take advantage of advances in U-Pb and U-series analytical techniques in an effort to make the long-sought chronology possible. For the Grand Canyon area (Fig. 2), there is no better niche than caves to find both clastic and chemical sediments that were deposited before, during, and after the incision of the canyon. Equally important, these cave deposits are located throughout the canyon. Caves are not only well suited to contain these deposits, they also provide an ideal environment that preserves and protects them from weathering. These mammillary coatings in the Grand Canyon caves contain sufficient uranium-lead ratios and yield U-Pb dates that place the water table within the canyon at a particular place and at an absolute time. This allows for the incision history of the Grand Canyon to be reconstructed

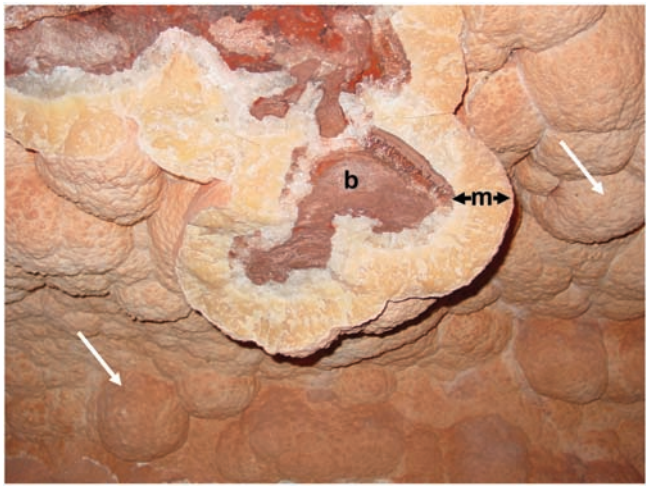

Fig. 1. Cave mammillaries coat cave walls below but near the water table. A cross section of broken mammillaries (m) and exposure of underlying bedrock (b) from site 6 (Tsean Bida) are shown. The unbroken form of this speleothem type (white arrows) indicates a subaqueous origin.

Department of Earth and Planetary Sciences, University of New Mexico, Albuquerque, NM 87131, USA.

*To whom correspondence should be addressed. E-mail: polyak@unm.edu